



1 **An ensemble estimate of Australian soil organic carbon**
2 **using machine learning and process-based modelling**

3
4 Lingfei Wang^{1,2}, Gab Abramowitz^{1,2}, Ying-Ping Wang³, Andy Pitman^{1,2} and Raphael A.
5 Viscarra Rossel⁴
6

7 ¹ ARC Center of Excellence for Climate Extremes, Sydney NSW 2052, Australia

8 ² Climate Change Research Center, University of New South Wales, Sydney NSW 2052, Australia

9 ³ CSIRO Environment, Private Bag 10, Clayton South VIC 3169, Australia

10 ⁴ Soil & Landscape Science, School of Molecular & Life Sciences, Faculty of Science & Engineering,
11 Curtin University, GPO Box U1987, Perth WA 6845, Australia.

12
13 Correspondence to: Lingfei Wang (lingfei.wang@unsw.edu.au)

14 **Abstract**

15
16 Spatially explicit prediction of soil organic carbon (SOC) serves as a crucial foundation for
17 effective land management strategies aimed at mitigating soil degradation and assessing carbon
18 sequestration potential. Here, using more than 1000 in-situ observations, we trained two
19 machine learning models (random forest, and K-means coupled with multiple linear
20 regression), and one process-based model (the vertically resolved Microbial-Mineral Carbon
21 Stabilization (MIMICS)) to predict SOC content of the top 30 cm of soil in Australia.
22 Parameters of MIMICS were optimized for different site groupings, using two distinct
23 approaches, plant functional types (MIMICS-PFT), and the most influential environmental
24 factors (MIMICS-ENV). We found that at the continental scale, soil bulk density and mean
25 annual temperature are the dominant controls of SOC variation, and that dominant controls vary
26 for different vegetation types. All models showed good performance in SOC predictions with
27 R^2 greater than 0.8 during out-of-sample validation with random forest being the most accurate,
28 and SOC in forests is more predictable than that in non-forest soils. Parameter optimization
29 approaches made a notable difference in the performance of MIMICS SOC prediction with
30 MIMICS-ENV performing better than MIMICS-PFT especially in non-forest soils. Digital
31 maps of terrestrial SOC stocks generated using all the models showed similar spatial
32 distribution with higher values in southeast and southwest Australia, but the magnitude of
33 estimated SOC stocks varied. The mean ensemble estimate of SOC stocks was 30.08 t/ha with
34 K-means coupled with multiple linear regression generating the highest estimate (mean SOC
35 stocks at 38.15 t/ha) and MIMICS-PFT generating the lowest estimate (mean SOC stocks at
36 24.29 t/ha). We suggest that enhancing process-based models to incorporate newly identified
37 drivers that significantly influence SOC variations in different environments could be key to
38 reducing the discrepancies in these estimates. Our findings underscore the considerable
39 uncertainty in SOC estimates derived from different modelling approaches and emphasize the
40 importance of rigorous out-of-sample validation before applying any one approach in Australia.

41
42



43 1. Introduction

44

45 Globally, the soil is the largest biogeochemically active terrestrial carbon pool, storing more
46 organic carbon than plants and the atmosphere combined. The turnover of soil organic carbon
47 (SOC) is a key function in plant growth, maintenance of soil water and nutrients, soil structure
48 stabilization and other biogeochemical processes (Lefèvre et al., 2017). Soil can act as either a
49 carbon sink or carbon source depending on the balance of carbon input through plant litter and
50 root exudates and output through respiration and leaching (Terrer et al., 2021; Panchal et al.,
51 2022). Even a small change in SOC stocks, in any direction, could significantly affect the
52 atmospheric concentration of CO₂ and thereby climate change (Stockmann et al., 2013).

53

54 Given the importance of SOC, there is now a large and growing interest in estimating spatially
55 explicit SOC content and stocks. SOC supports critically important soil-derived ecosystem
56 services, and the amount of SOC indicates the degree of land and soil degradation (Lorenz et
57 al., 2019). SOC content below a certain limit will lead to the decline of microbial diversity,
58 water holding capacity and soil productivity (Stockmann et al., 2015). Additionally, with
59 growing concerns about increasing anthropogenic CO₂ emissions, soil carbon sequestration has
60 emerged as a potential strategy for climate change mitigation (Smith, 2016; Rumpel et al.,
61 2018). Protection of existing SOC and rebuilding depleted stocks through land management are
62 potential strategies in mitigating climate change (Bossio et al., 2020). However, effective SOC
63 management requires accurate knowledge of its existing distribution. Reliable estimates of SOC
64 stocks and their spatial variation serve as a reference point for assessing how close soil is to its
65 maximum SOC storage capacity and its potential to sequester additional carbon (Six et al.,
66 2002; Georgiou et al., 2022). Precise estimation of contemporary SOC stocks also provides a
67 baseline map that can be used to calibrate and initialize dynamic-mechanistic models, enabling
68 the study of how SOC will respond to climate and land-use change (Minasny et al., 2013;
69 Viscarra Rossel et al., 2014). It is, for example, a prerequisite for accurately predicting future
70 carbon–climate feedbacks in Earth system models (ESMs) (Todd-Brown et al., 2013).

71

72 Accurately assessing SOC storage is challenging due to the complexity of carbon formation
73 and degradation processes in space and time (Keskin et al., 2019). Soil exists as a continuum
74 containing organic compounds at different stages of decomposition (Lehmann and Kleber,
75 2015). Soil formation can be described by a function of climate, organisms, relief, parent
76 material and time (Jenny, 1994). These factors are widely used in SOC studies for digital soil
77 mapping (McBratney et al., 2003; Viscarra Rossel et al., 2015; Liang et al., 2019). However,
78 the relationship between SOC storage and these driving variables is complex and spatially
79 variable (Mishra and Riley, 2015; Viscarra Rossel et al., 2019; Adhikari et al., 2020) leading to
80 substantial challenges and inherent uncertainties in SOC predictions.

81

82 Mechanistic process-based models and empirical models (including machine learning models)
83 are two widely employed approaches used to predict SOC stocks and their spatial distribution.
84 Conventional process-based models assume first-order kinetics for SOC decomposition,



85 wherein the rate of C decomposition is dependent on temperature and moisture but independent
86 of microbial biomass, and equilibrium SOC stock is proportional to carbon input and mean
87 residence time (Abs and Ferrière, 2020; Wang et al., 2021). ESMs coupled with conventional
88 SOC models cannot accurately predict patterns of contemporary soil carbon and show high
89 uncertainties in projected SOC dynamics under future climate change (Todd-Brown et al., 2013;
90 Todd-Brown et al., 2014). This is partly due to the lack of explicit representation of soil
91 microbial activities and metabolic traits (Wieder et al., 2015). Numerous microbial models have
92 been developed in the past few decades to improve model performance of SOC predictions
93 (Chandel et al., 2023), but these models has rarely been incorporated into large-scale modelling
94 frameworks partly due to the lack of rigorous validation (Luo et al., 2016). Process-based SOC
95 models are constructed based on our understanding on the major processes governing SOC
96 dynamics (e.g., carbon input, decomposition, and loss). However, the disagreement in
97 projections of carbon dynamics by different models highlights the need to improve our
98 knowledge of SOC cycling (Luo et al., 2016). Machine learning models without any process-
99 level assumptions provide a tool to identify the most influential controls on SOC variations.
100 Machine learning models can represent non-linear and non-smooth relationships between
101 predictor and response variables as well as interactions between different predictors (Heung et
102 al., 2016). Various machine learning algorithms have been successfully used in digital soil
103 mapping to predict high-resolution spatially explicit SOC content (Lamichhane et al., 2019).

104

105 Several modelling studies of soil carbon content/stocks have been conducted in Australia. Wang
106 et al. (2018a) trained boosted regression trees and random forest models using observations
107 from the semi-arid rangelands of eastern Australia. Both models predicted SOC stocks
108 moderately well based on performance metrics. The fitted models were then applied to map the
109 spatial distribution of SOC at two soil depths (0-5 cm and 0-30 cm). Continentally, Viscarra
110 Rossel et al. (2014) trained the CUBIST model, a form of piecewise linear decision tree, using
111 more than five thousand observations to produce a high resolution (90 m × 90 m) baseline map
112 of SOC stocks of Australian terrestrial systems and its uncertainty at 30 cm depth. Based on the
113 baseline map, Walden et al. (2023) derived spatially explicit estimates of Australian SOC stocks
114 and uncertainty including additional data from forests from southeastern Australia and coastal
115 marine (or blue carbon) ecosystems. SOC content at multiple soil depths along with associated
116 uncertainties were also estimated using different machine learning algorithms (Viscarra Rossel
117 et al., 2015; Wadoux et al., 2023). Moreover, the distribution of different soil carbon
118 compositions (i.e., the particulate, mineral-associated and pyrogenic organic carbon fractions)
119 and the importance of environmental factors on their variations were also studied using machine
120 learning (Viscarra Rossel et al., 2019). However, despite the progress made in SOC modelling,
121 significant uncertainties persist in SOC estimates due to the inherent complexities of SOC
122 variations, the lack of appropriately sampled SOC observations and the amount of data. All
123 these continental estimates were generated using empirical modelling approaches or first-order
124 biogeochemical models (Grace et al., 2006; Lee et al., 2021). Estimates from mechanistic SOC
125 models with explicit representation of microbial metabolism are missing despite offering the



126 potential to better constrain SOC dynamics under future climate change scenarios in a way that
 127 empirical approaches cannot.

128

129 Our primary objective in this paper is to assess the predictability of SOC stocks in Australia.
 130 We generate a range of estimates of terrestrial SOC stocks, employing both process-based and
 131 empirical modelling, and examine why these estimates might differ. First, we discern the
 132 significance of environmental predictors, both at continental and biome scales. We then
 133 evaluate the performance of random forests, k-means with multiple linear regression and the
 134 vertically resolved MICrobial-MIneral Carbon Stabilization (MIMICS) SOC model with
 135 different parametrization approaches. Finally, we compare the spatial estimates of SOC stocks
 136 using these different approaches across Australia, and discuss their differences and potential
 137 application to future SOC projection.

138

139 2. Materials and Methods

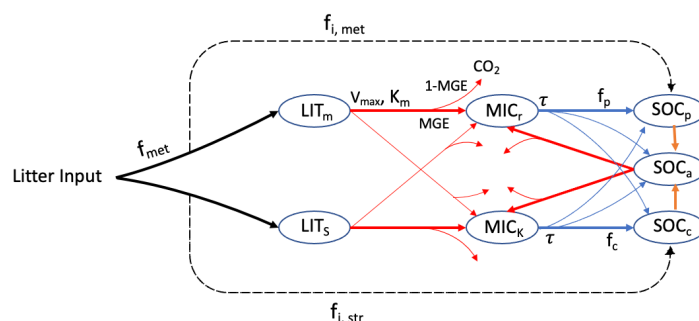
140 2.1. Model descriptions

141 2.1.1. Vertically resolved MIMICS

142

143 The MICrobial-MIneral Carbon Stabilization (MIMICS) model (Wieder et al., 2015; Zhang et
 144 al., 2020) is a soil carbon model that explicitly considers relationships between litter quality,
 145 functional trade-offs in microbial physiology, and the physical protection of microbial by-
 146 products in forming stable soil organic matter. There are two litter pools: metabolic (LIT_m) and
 147 structural (LIT_s) litter (Figure 1), and the partitioning of litter input into metabolic and structural
 148 pools is determined by the chemical properties of the litter. Litter and SOC turnover are
 149 governed by two microbial functional types that exhibit copiotrophic (i.e., r-selected, MIC_r) and
 150 oligotrophic (i.e., K-selected, MIC_k) growth strategies. The MIC_r is assumed to have higher
 151 growth and turnover rates, and a preference for consuming labile litter (LIT_m), while MIC_k
 152 is characterized by lower growth and turnover rates, and a greater competitive advantage when
 153 consuming low-quality litter (LIT_s) and chemically recalcitrant SOC. SOC in MIMICS is
 154 divided into three pools: physically protected (SOC_p), (bio)chemically recalcitrant (SOC_c) and
 155 available (SOC_a) carbon (Figure 1).

156



157

158 **Figure 1.** Soil carbon pools and fluxes represented in MIMICS (adapted from Wieder et al., (2015)). Litter
 159 inputs are partitioned into metabolic and structural litter pools (LIT_m and LIT_s) based on litter quality (f_{met}).



160 Decomposition of litter and available SOC pool (SOC_a) are governed by temperature sensitive Michaelis-
161 Menten kinetics (V_{\max} (maximum reaction velocity) and K_m (half saturation constant)), shown by red lines.
162 Microbial growth efficiency (MGE) determines the partitioning of C fluxes entering microbial biomass pools
163 vs. heterotrophic respiration. Turnover of microbial biomass (τ , blue) depends on microbial functional types
164 (MIC_r and MIC_k), and is partitioned into available, physically protected and chemically recalcitrant SOC
165 pools (SOC_a , SOC_p and SOC_c , respectively).
166

167 The decomposition of litter pools and SOC pools follows temperature-sensitive Michaelis-
168 Menten kinetics. Microbial growth efficiency (MGE) determines the partitioning of carbon
169 fluxes entering microbial biomass pools (MIC_r and MIC_k) versus heterotrophic respiration.
170 Access of microbial enzymes to available substrates is restricted by soil texture. The equations
171 of MIMCS are from Wieder et al. (2015), except that the density-dependent microbial turnover
172 was introduced to MIMCS to minimize an unrealistic oscillation (Zhang et al., 2020). To better
173 simulate carbon turnover at different soil depths, vertical transport of soil carbon was introduced
174 into MIMICS considering carbon transported through bioturbation and diffusion among
175 adjacent soil layers (Wang et al., 2021).
176

177 Vertically resolved MIMICS is run using a daily time step. The soil was divided into 15 layers,
178 each of 10 cm thickness. All the sites in this study are assumed to be at steady state (i.e., no
179 interannual variation of SOC). Historical climate, litterfall input and soil properties were all
180 assumed to be similar to the average conditions. At each site, the pool size was initialized within
181 a sensible range for different pools and spun up to finally achieve steady state.
182

183 2.1.2. Machine learning

184

185 Two machine learning algorithms were applied in this study to predict SOC. First, random forest
186 (RF) is a tree-based ensemble learning method that works by building a set of regression trees
187 and averaging results (Breiman, 2001). Within the training procedure, the RF algorithm
188 produces multiple trees. Each regression tree in the forest is independently constructed based
189 on a unique bootstrap sample (with replacement) from the original training data set. The
190 response, as well as the predictor variables are either categorical (classification trees) or
191 numeric (regression trees). Bootstrap sampling makes RF less sensitive to overfitting and
192 allows for robust error estimation based on the remaining test set, the so-called Out-Of-Bag
193 (OOB) sample (Wiesmeier et al., 2014). We used the “ranger” package R (version 4.2.0) for RF
194 computation. We trained the RF model with different numbers of trees and observed that the
195 model's performance remained similar regardless of the number of trees used. The number of
196 regression trees generated in the forest (num.trees) was finally set as 200, and the number of
197 predictors randomly selected at each node (mtry) was set as default, which was 2.
198

199 Multiple linear regression (MLR) is widely used in SOC studies but found to be less effective
200 than machine learning algorithms (Lamichhane et al., 2019). Here, instead of applying MLR
201 directly with all environmental factors as predictors, our approach involved a preliminary step
202 where we partitioned all observations into distinct clusters using K-means, an unsupervised



203 machine learning algorithm. K-means aims to segregate the data into a predefined number of
204 clusters (k), with the objective of maximizing the similarity among data within each cluster.
205 The underlying assumption here was that sites sharing similar environmental conditions would
206 exhibit comparable SOC concentration. In cases where certain clusters had fewer observations
207 than five times the number of predictors, we augmented these clusters by incorporating
208 observations from other clusters. This augmentation process was guided by the Euclidean
209 distance between the observation and the cluster centre, ensuring a more robust construction of
210 the linear regression model. To determine the number of clusters, we applied the coupled K-
211 means and MLR with varying number of clusters. The selection of the optimal number of
212 clusters was based on the criterion of producing the smallest root mean square error during
213 independent out-of-sample validation.

214

215 2.2. Identification of dominant controllers on SOC concentration

216

217 RF-based measures of variable importance have gained widespread popularity as tools for
218 evaluating the contributions made by predictor variables within a fitted random forest model
219 (Debeer and Strobl, 2020). In the context of this study, we employed permutation variable
220 importance (PVI) within the random forest framework to gauge the significance of predictors
221 in predicting SOC concentration.

222

223 The permutation variable importance entails measuring the reduction in a RF model's
224 performance score upon random shuffling of a single variable values. By doing so, the inherent
225 relationship between the variable and the SOC concentration is disrupted. Consequently, the
226 disparity in prediction accuracy observed in a random forest model before and after such
227 shuffling serves as a quantitative representation of the significance of the particular predictor
228 in predicting SOC concentration. The greater the importance of the predictor, the higher its
229 corresponding PVI value becomes.

230

231 2.3. Parameter optimization

232

233 MIMICS parameters were derived from (Zhang et al., 2020; Wang et al., 2021), except that five
234 parameters (Table 1) which directly control the organic carbon decomposition were optimized.
235 An effective global optimization algorithm called the shuffled complex evolution (SCE-UA,
236 version 2.2) method (Duan et al., 1993) was applied for parameter optimization. Parameters
237 were optimized by minimizing the sum of squared residuals between the observed and modelled
238 values.

239

240 Vertically resolved MIMICS simulated SOC concentration for 15 soil layers. As observations
241 only provide one measurement for the top 30 cm soil, we computed the average of the modelled
242 values spanning the 0-10 cm, 10-20 cm, and 20-30 cm soil layers. This average was then
243 adopted as the modelled SOC concentration for top 30 cm soil, serving as the basis for
244 evaluating the difference between observations and simulations.

245



246 **Table 1.** The optimized model parameters and their value range

Parameter	Definition	Range
a_v	A scaling factor for V_{max}	0-30
a_k	A scaling factor for K_m	0-20
x_{desorp}	A scaling factor for SOC desorption rate	0-3
x_{beta}	An exponent of the biomass density dependent mortality rate of microbes	1.05-2
$x_{diffsoc}$	A scaling factor for SOC diffusion coefficient in soil	0-30

247

248 Parameters were optimized for distinct groups divided based on two approaches. The first
 249 approach involved categorizing all observations into four groups based on plant functional
 250 types (PFTs). The second approach was taking the most influential abiotic variables as
 251 predictors (as outlined in Section 2.2) and dividing all observations into 6 clusters using the K-
 252 means algorithm. The determination of the optimal number of clusters was achieved through
 253 the minimization of the sum of the within-cluster-sum-of-squares-of-all-clusters (WCSSE), a
 254 process facilitated by the "ClusterR" package in R (version 4.2.0). This clustering aimed to
 255 ensure the highest possible similarity among the environmental factors within each cluster. It
 256 was anticipated that SOC ranges within each cluster would be narrow due to the high similarity
 257 of environmental predictors.

258

259 2.4. Data

260 2.4.1. Predictors of SOC concentration

261

262 MIMICS requires gridded mean annual temperature (MAT), carbon input and clay content as
 263 driving variables for a spatial simulation. Soil bulk density is also required for conversion
 264 between SOC concentration (g C/kg soil) and SOC stocks (t/ha). Gridded mean annual
 265 precipitation (MAP) and vegetation types were also used during calibration and when
 266 understanding the drivers and spatial variability of SOC. Details of gridded data can be found
 267 in Table 2.

268

269 Gridded daily maximum temperature, minimum temperature, and precipitation at 0.05°
 270 resolution were obtained from the SILO database of Australian climate data. Mean daily
 271 temperature was approximated as the average of maximum and minimum daily temperature.
 272 MAT was calculated from mean daily temperature from 1991 to 2020, and MAP was calculated
 273 from daily precipitation from 1991 to 2020.

274

275 Carbon input was represented by NPP. Gridded mean annual NPP at 500 m was calculated
 276 based on annual NPP from 2001 to 2020 obtained from MODIS (MOD17A3HGF V6.1). NPP
 277 was partitioned to above-/belowground part by multiplying by the root/shoot ratio for different
 278 vegetation types (Mokany et al., 2006).

279

280 The distribution of vegetation types at 3'' resolution was obtained from National Vegetation
 281 Information System (NVIS, version 6.0). Pixels of non-vegetated regions were removed and
 282 types were aggregated to just 4 PFTs: forest, woodland, shrubland and grassland.

283



284 Soil bulk density and clay content were obtained from Soil and Landscape Grid National Soil
 285 Attributes Maps (SLGA – Release 2). Soil properties were predicted based on machine learning
 286 at depths 0-5 cm, 5-15 cm, 15-30 cm, 30-60 cm, 60-100 cm, and 100-200 cm in SLGA. Bulk
 287 density and clay content were estimated for top 30 cm soil as weighted average of first 3 layers
 288 in SLGA.

289

290 The initial spatial resolution of the gridded data was maintained when extracting the required
 291 environmental factors for each SOC observation. All data were then resampled to 0.05°
 292 resolution using bilinear interpolation for estimation of terrestrial SOC stocks at continental
 293 scale.

294

295 **Table 2.** Information of gridded data used in this study.

	Source	Spatial Scale	Temporal Scale	Unit	Time Period	Ref.
Maximum Temperature	SILO	~5 km	daily	°C	1991-2020	(Jeffrey et al., 2001)
Minimum Temperature	SILO	~5 km	daily	°C	1991-2020	(Jeffrey et al., 2001)
Precipitation	SILO	~5 km	daily	mm	1991-2020	(Jeffrey et al., 2001)
NPP	MODIS	500 m	annually	g C/m ²	2001-2020	(Running and Zhao, 2021)
Vegetation Types	NVIS	100 m	/	/	/	
Soil Bulk Density	SLGA	~90 m	/	kg/m ³	/	(Grundy et al., 2015; Viscarra Rossel et al., 2015)
Soil Clay Content	SLGA	~90 m	/	%	/	(Grundy et al., 2015; Viscarra Rossel et al., 2015)

296

297 2.4.2. Soil organic carbon observations

298

299 SOC observations for top 30 cm soil in Australia were collected from two datasets. The first
 300 one, VR dataset, is described in (Viscarra Rossel et al., 2014; Viscarra Rossel et al., 2019). We
 301 removed the observations collected from croplands based on the land-use record in the dataset
 302 and removed those from unvegetated regions based on NVIS vegetation map (see above).
 303 Observations at 1070 sites remained. SOC stocks were reported in t/ha and converted to SOC
 304 concentration (g C/kg soil) using soil bulk density (BD, kg/m³) and soil depth (m),

305

$$306 \quad SOC_{concentration} = SOC_{stock} / (BD \times depth) \times 100 \quad (1)$$

307

308 Clay content and soil bulk density were reported in this dataset and also in Viscarra Rossel et
 309 al. (2015). To better represent SOC distribution in forest, we obtained more forest SOC
 310 observations from a second dataset, the Biomes of Australian Soil Environments (BASE)
 311 described in (Bissett et al., 2016). Here, SOC concentration was reported for 0-10 and 20-30
 312 cm, and we estimated the SOC concentration for 20-30 cm soil using the algorithm (Jobbágy
 313 and Jackson, 2000) below,

314

$$315 \quad \log_{10} C = S \log_{10} d + I \quad (2)$$

316



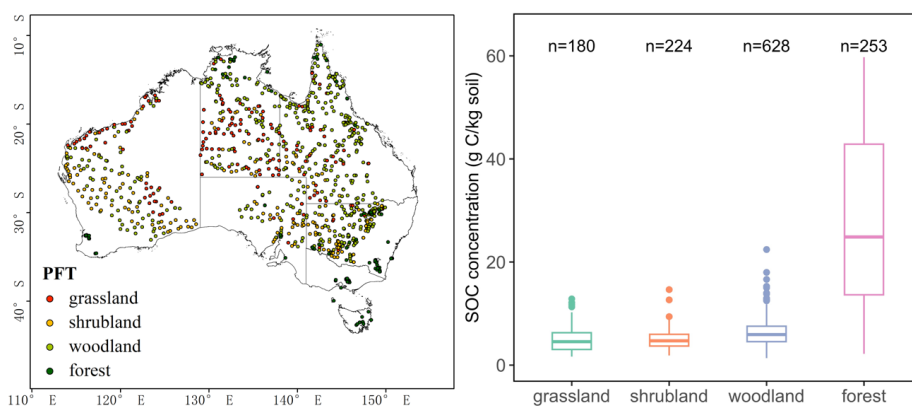
317 Where C represents the SOC stocks (t/ha), and d represents depth. S and I are parameters of the
 318 model. We took the average SOC concentration of three layers as the value for top 30 cm soil.
 319 Clay content was reported in this dataset and bulk density was extracted from SLGA (see
 320 above).

321

322 The spatial distribution of SOC concentration observations from different PFTs is shown in
 323 Figure 2a. SOC concentration in top 30 cm is positively skewed, ranging from 1.36 to 59.73 g
 324 C/kg soil with mean value at 9.97 g C/kg soil and median value at 6.11 g C/kg soil. SOC
 325 concentration in grassland, shrubland and woodland show similar distribution patterns (Figure
 326 2b), while SOC concentration in forest is more variable with a standard deviation at 15.92 g
 327 C/kg soil.

328

329



330

331

332 **Figure 2.** Spatial distribution of 1285 soil organic carbon concentration observations used in this study and
 333 the plant functional types which they belong to (a); boxplots of SOC concentration distributions for each
 334 plant functional type (b). For boxplots, centre lines represent the median value, and upper and lower box
 335 boundaries represent third and first quartile. Whiskers extend to the smallest and largest values within 1.5
 336 times the interquartile range.

337

338 2.5. Model evaluation

339

340 For machine learning models, all observations were separated to a training and test dataset
 341 randomly with 70% used to train the model and the remaining 30% used to validate the
 342 predictions of SOC concentration. For vertically resolved MIMICS, parameters were optimized
 343 for each group, and we again randomly selected 70% of observations in each group to train the
 344 model and used the remaining 30% for validation. To cross-validate, the procedure was repeated
 345 10 times.

346

347 The performance of models was evaluated using four metrics. Mean Absolute Error (MAE)
 348 indicates how close the average predictions are to average observations. Root Mean Square
 349 Error (RMSE) measures the overall accuracy combining mean, standard deviation differences



350 (across sites) and (spatial) correlation. Coefficient of determination (R^2) measures the
 351 percentage of variation explained by the model. Lin's Concordance Correlation Coefficient
 352 (LCCC) (Lawrence and Lin, 1989) measures the level of agreement between predictions and
 353 observations following the 1:1 line. A good model will have MAE and RMSE close to 0 and R^2
 354 and LCCC close to 1.

355

356 2.6. Estimation of terrestrial SOC stocks

357

358 To examine terrestrial SOC stocks and their continental-scale spatial distribution, we generated
 359 pixel-based SOC maps utilizing the four models validated within this study. In the cases of
 360 MIMICS-PFT and MIMICS-ENV, the initial step involved segregating all pixels into four
 361 distinct plant functional groups or six environmental clusters. Since cross-validation was
 362 performed, the machine learning and process-based models were evaluated using test data, and
 363 the models with the optimal performance were subsequently employed at each pixel to estimate
 364 terrestrial SOC stocks. The map of ensemble estimate of SOC stocks was also produced as the
 365 average of four models at each pixel.

366 3. Results

367

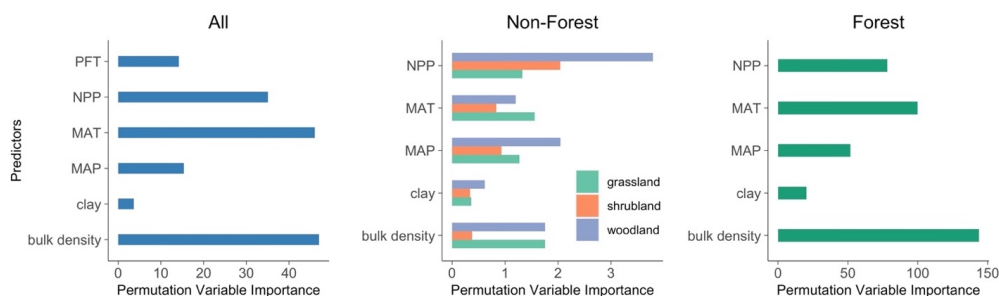
368 3.1. Dominant environmental controls of SOC concentration

369

370 Using the Permutation Variable Importance (PVI) in random forest, we identified the
 371 significance of environmental factors in predicting SOC. At the continental scale, soil bulk
 372 density is the most influential driver of SOC concentration variations, following by MAT, NPP
 373 and MAP (Figure 3). Soil clay content and plant functional type exhibit relatively lesser
 374 significance in this regard.

375

376 The relative predictor importance for forests and grasslands aligns with the importance at
 377 continental scale. In shrubland and woodland, NPP and MAP emerge as the pivotal factors.
 378 Collectively, across both continental and regional scales, soil bulk density, MAT, and MAP are
 379 the three most influential abiotic factors.



380

381

Figure 3. Importance of predictors on SOC concentration for different plant functional types.



382 3.2. Data clustering based on environmental factors

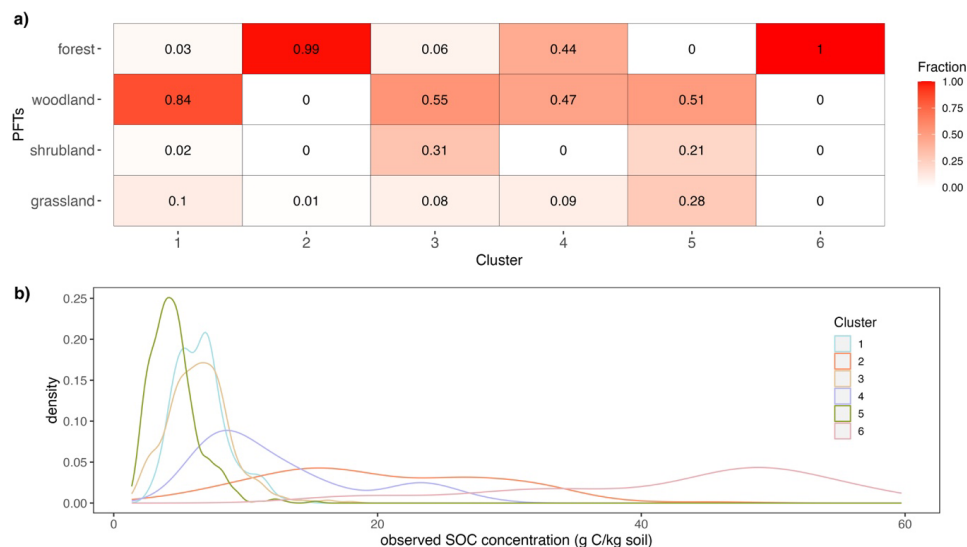
383

384 To develop the calibration groups for MIMICS-ENV, we partitioned the top three important
385 abiotic factors, which are soil bulk density, MAT and MAP, into six distinct clusters using K-
386 means (see Section 2.3). The resulting characteristics and SOC distributions for these six
387 clusters are illustrated in Figure 4.

388

389 Notably, a substantial majority of forests were assigned to clusters 2 and 6 (Figure 4a), while
390 woodland, shrubland, and grassland observations were distributed across the remaining four
391 clusters. Among these clusters, cluster 5 exhibits the lowest SOC concentration, while SOC of
392 cluster 1 and 3 display a comparable pattern but spread across different biomes. Conversely,
393 distribution of SOC concentration in clusters 2, 4, and 6 shows more pronounced variability
394 (Figure 4b).

395



396

397 **Figure 4.** Fraction of different PFTs in each cluster divided based on environmental factors (a) and density
398 plot of observed SOC concentration for different clusters (b).

399

400 3.3. Evaluation of model performance

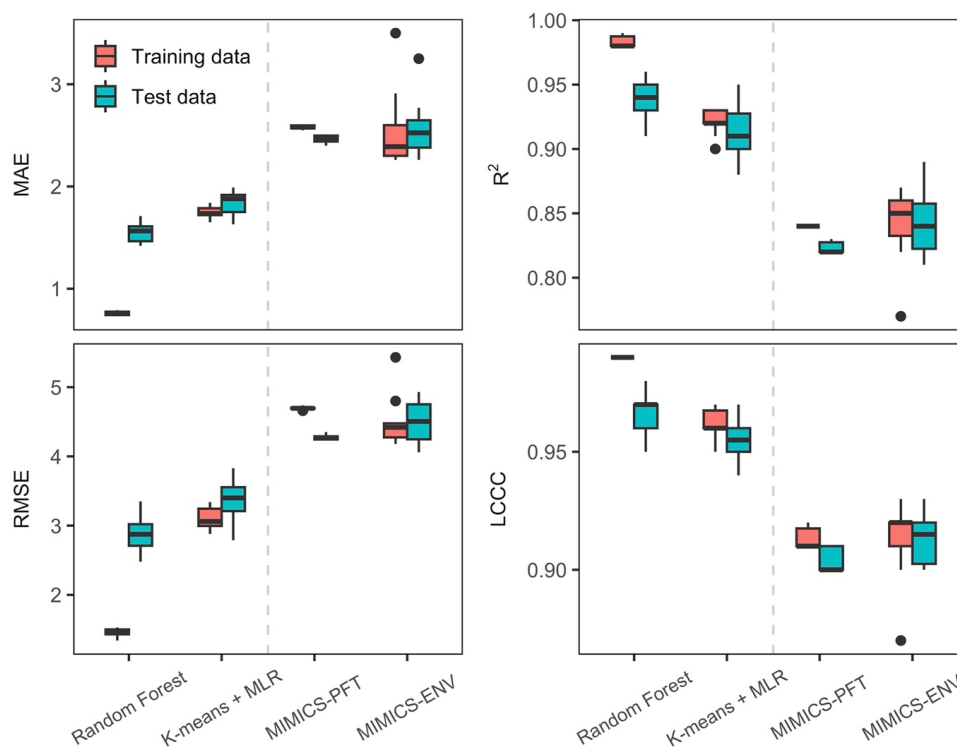
401

402 All models employed in this study (RF, K-means + MLR, MIMICS-PFT and MIMICS-ENV)
403 predicted SOC concentration well for both training data and test data (Figure 5). As anticipated,
404 performance for both process-based model and machine learning models degrade using out-of-
405 sample data versus in-sample training or calibration data. When using test data, the mean value
406 of R^2 for all models ranges from 0.82 to 0.94, mean LCCC ranges from 0.90 to 0.97, mean
407 RMSE ranges from 2.88 to 4.51 g C/kg soil, and mean MAE ranges from 1.55 to 2.57 g C/kg
408 soil.

409



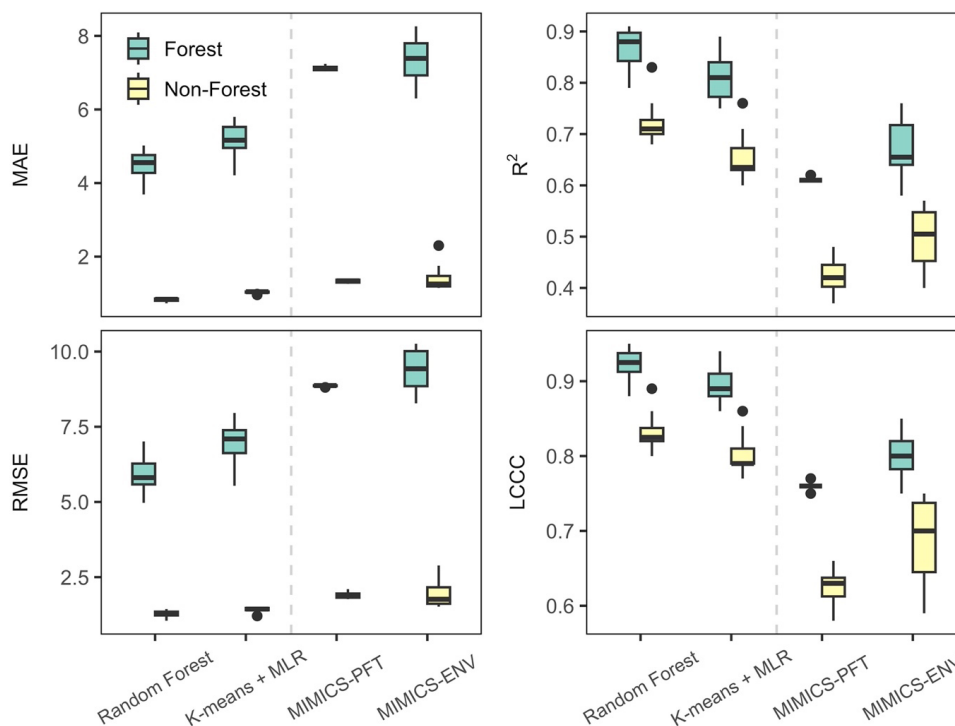
410 The machine learning models outperformed MIMICS in predicting SOC concentration,
 411 regardless of the optimisation approach taken. Particularly, the random forest algorithm
 412 demonstrated the most accurate predictions characterized by higher R^2 and LCCC values and
 413 lower RMSE and MAE values for both training and test data. While MIMICS-ENV displayed
 414 performance similar to that of MIMICS-PFT in SOC concentration predictions based on RMSE
 415 and MAE, the former exhibited slightly superior median R^2 and LCCC values (Figure 5).



416
 417 **Figure 5.** Performance metrics of SOC concentration predictions. Units for MAE and RMSE are g C/kg.
 418 Centre line represents median value, and upper and lower box boundaries represent third and first quartile.
 419 Whiskers extend to the smallest and largest values within 1.5 times the interquartile range.

420
 421 SOC concentration in forest soil exhibited significantly higher predictability than those in non-
 422 forest (woodland, shrubland and grassland) soil, evidenced by higher R^2 (ranging from 0.58 to
 423 0.91) and LCCC (ranging from 0.75 to 0.95) for test data (Figure 6). Machine learning
 424 algorithms surpassed MIMICS in predicting SOC for both forest and non-forest soils. Notably,
 425 MIMICS-ENV outperformed MIMICS-PFT in SOC predictions, particularly in non-forest
 426 soils.

427
 428



429

430

431 **Figure 6.** Performance metrics of SOC concentration predictions for forest and non-forest (woodland, shrubland and grassland) soils in test (out-of-sample) data. Unit for MAE and RMSE is g C/kg soil. Centre

432 line represents median value, and upper and lower box boundaries represent third and first quartile. Whiskers

433 extend to the smallest and largest values within 1.5 times the interquartile range.

434

435

436 3.4. Estimations of terrestrial SOC stocks

437

438 Descriptive statistics of predicted terrestrial SOC stocks at 0-30 cm soil depth are shown in

439 Table 3. Forests have the largest mean SOC stocks ranging from 70.3 to 113.9 t/ha by all models,

440 and shrubland is estimated to have the lowest mean SOC stocks. The distributions of predicted

441 continental SOC stocks by all models are positively skewed with most estimated SOC stocks

442 less than 50 t/ha (Figure 7a), and SOC stocks at peak density predicted by MIMICS-ENV and

443 MIMICS-PFT are smaller than those predicted by machine learning approaches. The maximum

444 value of SOC stocks predicted by all models vary considerably.

445

446 As expected, all models consistently projected greater SOC stocks in the southeast region,

447 southwest corner and Tasmania, and consistently indicated lower SOC stocks in central and

448 western Australia (Figure 7b). Notably, MIMICS-ENV depicted a pronounced deficit of SOC

449 in central Australia, a distinctive pattern compared to the predictions of other models. Among

450 the models, K-means coupled with multiple linear regression consistently provided the highest

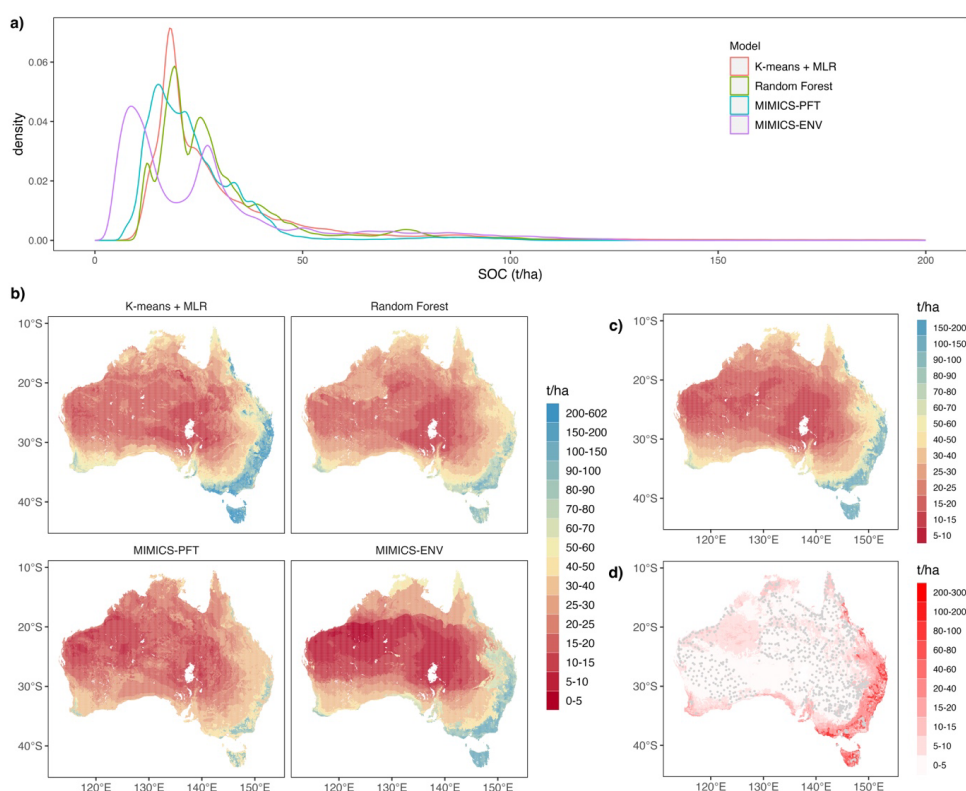
451 SOC estimations across all vegetation types, while MIMICS-PFT model consistently yielded

452 the lowest mean SOC stocks.



453

454 The ensemble estimate of SOC stocks (Figure 7c) shows a similar distribution pattern as that
 455 generated by single approach. The SOC stocks of the ensemble range from 9.3 to 180.4 t/ha
 456 with an average value of 30.1 t/ha. The standard deviation across the four estimates (Figure
 457 7d) is positively correlated with the ensemble mean estimate. That is, soils with higher SOC
 458 stocks exhibit greater variability in SOC predictions among different models. Note also that the
 459 variability of estimates tends to be smaller in areas with denser numbers of observations.
 460



461

462

463 **Figure 7.** Predicted Australian terrestrial SOC stocks (t/ha) for top 30 cm soil and ensemble statistical
 464 characteristics: a) density plot of estimated terrestrial SOC stocks by all models, noting that only stocks less than
 465 200 t/ha are shown for better comparison of the distribution; b) Predicted SOC stocks for each model;
 466 c) Predicted SOC stocks of the ensemble; d) standard deviation stocks within the ensemble. Grey points
 467 represent locations of SOC observations.

468

469

470

471

472

473

474



475 **Table 3.** Descriptive statistics of predicted terrestrial SOC stocks (t/ha) at 0-30 cm soil. Min. and Max. are
 476 minimum and maximum value, respectively. 1st Qu and 3rd Qu are first and third quartile, respectively.
 477

	PFT	Min.	1 st Qu	median	mean	3 rd Qu	Max.
K-means + MLR	grassland	4.2	17.9	21.2	41.5	42.5	601.1
	shrubland	7.2	16.4	19.3	23.6	24.4	472.2
	woodland	7.1	20.1	26.1	33.3	33.7	483.1
	forest	18.0	51.3	95.2	113.9	153.4	474.0
	all	4.2	18.1	23.6	38.2	16.7	601.1
Random Forest	grassland	10.4	18.5	26.0	30.4	37.2	125.3
	shrubland	10.3	17.0	19.6	21.4	24.4	104.4
	woodland	10.5	20.3	25.8	28.2	32.4	122.1
	forest	29.3	55.0	82.3	78.4	97.0	161.7
	all	10.3	18.9	25.0	29.8	33.7	161.7
MIMICS- PFT	grassland	10.8	16.4	24.1	25.1	33.3	58.7
	shrubland	6.5	12.2	15.5	16.5	20.6	56.5
	woodland	7.8	17.4	21.2	22.1	25.9	61.4
	forest	17.9	44.5	77.4	70.3	88.5	109.9
	all	6.5	15.7	21.2	24.3	28.9	109.9
MIMICS- ENV	grassland	4.2	7.9	15.4	26.9	37.6	124.0
	shrubland	4.4	9.9	13.4	18.6	25.3	131.9
	woodland	4.9	14.7	26.3	28.4	31.3	131.6
	forest	9.6	53.1	92.4	81.6	106.5	134.1
	all	4.2	10.5	21.9	28.1	33.2	134.1

478

479 4. Discussion

480 4.1. Relative importance of predictors on SOC variations

481

482 Extensive research has been conducted to discern the factors that govern SOC content/stocks.
 483 Among the commonly employed predictors for SOC variations, climate, organisms,
 484 topography, parent material, and soil properties are prominent (Wiesmeier et al., 2019). Within
 485 this study, we conducted a comparative assessment of the significance of key variables, namely
 486 MAT, MAP, NPP, soil clay content and bulk density, in driving variations in SOC in Australia.
 487 While the number of predictors utilized in our approach is fewer than that employed in most
 488 digital mapping methodologies, its strength lies in the potential for a more direct comparison
 489 between empirical and process-based models.

490

491 Soil bulk density is the most important driver of SOC concentration at the continental scale
 492 (Figure 3). The role of soil bulk density in SOC has been noted before in eastern Australia
 493 (Hobley et al., 2015). Soil bulk density is mainly a function of the parent material, soil genesis
 494 as well as soil aggregate formation (Don et al., 2007). A soil with reduced density exhibits
 495 superior structural organization and an expanded surface area, facilitating enhanced retention
 496 of organic carbon (Lobsey and Viscarra Rossel, 2016). Subsequently, with a slightly lower value
 497 of importance than soil bulk density, MAT emerges as the second most influential factor
 498 governing SOC variations, followed by NPP, MAP, and clay content. This sequence of
 499 significance diverges from the findings of Walden et al. (2023), where the order of importance
 500 was observed as NPP > clay content > MAP > MAT on a continental scale in Australia. The



501 number of predictors used in their study is much more than that in our study, which may affect
502 the contribution of given predictors in SOC variation (Guo et al., 2019). This discrepancy might
503 however be attributable to the utilization of observations encompassing both terrestrial and blue
504 carbon ecosystems in their study. Clay emerges as key driver mainly in the groups where aquatic
505 plants (e.g., seagrass, tidal marsh) appeared. The more extensive dataset encompassing the
506 eastern coastline, characterized by greater variability and abundance of NPP input, potentially
507 elevates NPP to a dominant role in influencing SOC variations within their study.

508

509 For SOC in different vegetation types (Figure 3), soil bulk density and MAT are more important
510 than other factors in forest, and all factors except clay content showed similar importance in
511 driving SOC in grassland. NPP and MAP dominate the SOC variations in woodland and
512 shrubland. Climate conditions exert their impact on SOC in all vegetation types. It was proposed
513 that the primary climatic determinant of SOC variation hinges on the primary constraint
514 affecting SOC production and turnover (Hobley et al., 2016). In this study, most shrublands and
515 woodlands are distributed in arid and semi-arid regions characterized by limited precipitation,
516 which leads to water stress in surface soil, limiting plant productivity and reducing soil C input
517 (Hobley et al., 2015). Consequently, MAP and NPP exhibited relatively higher influence on
518 SOC variations. In contrast, forest SOC observations are mainly distributed in areas with
519 relatively lower temperatures, therefore experience constrained microbial metabolism, leading
520 to reduced decomposition rates and the high accumulation of SOC (Wynn et al., 2006).
521 Consequently, MAT emerges as a key factor influencing SOC variations in forests. Furthermore,
522 it is noteworthy that soil bulk density plays a crucial role in determining SOC distribution within
523 forest ecosystems, where it is significantly lower compared to other vegetation types. This
524 lower soil bulk density likely facilitates the formation of microaggregates and enhances the
525 preservation of SOC within the soil matrix (Bronick and Lal, 2005). Consequently, it effectively
526 contributes to elevated SOC concentration levels in forested areas.

527

528 PFTs are the only categorical predictor for SOC concentration in this study. SOC is mainly
529 derived from plant C input through above-/belowground tissues, and SOC turnover and storage
530 are influenced by plant traits like plant growth rate and chemical and physical composition (De
531 Deyn et al., 2008; Faucon et al., 2017). With shared representation of similar plant traits, PFTs
532 are widely used in process-based models (Poulter et al., 2015; Famiglietti et al., 2023). It was
533 found that the vertical distribution of SOC is highly related to PFTs due to the different root
534 distribution and above- and belowground allocation (Jobbágy and Jackson, 2000). However,
535 our study is limited by the absence of SOC observations at multiple soil depths, restricting the
536 analysis to the spatial distribution of SOC at 30 cm soil depth. The influence of PFTs on SOC
537 concentration at this particular depth appears relatively insignificant (Figure 3), casting doubt
538 on the effectiveness of optimizing parameters of process-based model for individual PFTs
539 (Cranko Page et al., 2023). Considering this, employing the top 3 influential abiotic predictors,
540 soil bulk density, MAT, and MAP, we partitioned all observations into six distinct clusters using
541 K-means. It was anticipated that SOC ranges within each cluster would be narrow due to the
542 high similarity of these three predictors within each group. However, the distribution of SOC



543 in clusters 2, 4, and 6 exhibited considerable variability (Figure 4). Given that these clusters are
544 predominantly composed of forest ecosystems, it becomes apparent that these three abiotic
545 factors alone are insufficient to fully characterize the intricacies of forest SOC concentration. It
546 was found that elevation and evapotranspiration also drive the variation of forest SOC in
547 Australia (Walden et al., 2023), and taking them into account might potentially increase the
548 predictability of forest SOC.

549

550 4.2. Model evaluation and comparison

551

552 Although the predictors used for machine learning models are not exactly same as the inputs of
553 MIMICS, the missing factors (e.g., MAP) were used for parameter optimization of MIMICS-
554 ENV, making the predictions dependent on similar information and so comparable to some
555 extent. Besides, our study presented clear evaluation metrics for out-of-sample validation,
556 enabling a more robust assessment of model performance when applied to new datasets.

557

558 Based on the performance metrics of test data, the machine learning models performed
559 remarkably well (Figure 5). The R^2 suggest that both two machine learning models can explain
560 more than 90% of SOC variability across sites, and random forest did the best job with greatest
561 R^2 and LCCC, and lowest MAE and RMSE. Random forest algorithms were widely adopted in
562 predicting spatial-temporal SOC dynamics and produced moderate well performance regionally
563 and globally. For example, Wang et al. (2022) applied random forest to estimate SOC stocks in
564 south-eastern Australia and explained 69% of the variation of current SOC stocks. Nyaupane et
565 al. (2023) trained a random forest model using global SOC observations and explained 61% of
566 SOC variation. The good performance of random forest might be attributed to reduced
567 susceptibility to over-fitting and better capacity to manage the hierarchical non-linear
568 relationships that exist between SOC and environmental predictors (Wang et al., 2018b). Other
569 machine learning methods have been applied to predict continental SOC stocks in Australia.
570 For example, Walden et al. (2023) trained regression-tree algorithm CUBIST to predict SOC
571 stocks at 30 cm soil using the harmonised datasets. The mean LCCC and RMSE for out-of-
572 sample validation in their study was 0.78 and 0.20 respectively when \log_{10} transformed SOC
573 (t/ha) values used. Wadoux et al. (2023) applied quantile regression forest to predict SOC stocks
574 at multiple soil depths. The prediction accuracy decreased dramatically for deeper depth
575 intervals with the greatest R^2 (0.53) at 0-5 cm soil. The better results in this study may be
576 attributed to the removal of cropland ecosystems, which are clearly highly managed and so less
577 predictable. Agricultural practices greatly affect SOC content in Australia and add the
578 complexity to the relationship between SOC and environmental factors (Luo et al., 2010).
579 Models using environmental predictors without representation of land use management are
580 unlikely to be able to fully capture the SOC dynamics in croplands (Abramoff et al., 2022).

581

582 Although MIMICS made less accurate estimations of SOC than machine learning models, it
583 did well at continental scale with mean R^2 at 0.82 and 0.84 for MIMICS-PFT and MIMICS-
584 ENV, respectively (Figure 5). Georgiou et al. (2021) found that there was a mismatch between



585 observations and MIMICS in the role of environmental controls in explaining SOC variability
586 at global scale. NPP and MAT had the most explanatory power for SOC stocks from MIMICS,
587 while clay content had the most explanatory power for SOC observations, which limits the
588 predictability of SOC using MIMICS in their study. However, in our study, NPP and MAT rather
589 than clay content played a greater role in observed SOC variations, perhaps contributing to a
590 better performance of MIMICS in Australia. The modest performance of MIMICS relative to
591 machine learning models could potentially be attributed to the absence of explicit representation
592 of MAP. The augmentation of MAP within parameter optimization in MIMICS-ENV did allow
593 improved performance compared to MIMICS-PFT, particularly within non-forest regions
594 where the importance of MAP rivals or surpasses that of temperature. Precipitation is a
595 determinant of plant productivity, especially in arid and semi-arid regions. Besides, arid regions
596 with limited precipitation are characterized by lower weathering rate limiting the formation of
597 mineral-associated soil carbon (Doetterl et al., 2015). Hence, we assume that introducing the
598 effect of moisture to MIMICS could contribute to more accurate prediction of SOC, as
599 compared with just taking MAP into account for parametrization, especially in arid and
600 semiarid regions.

601

602 All models produced lower MAE and RMSE for non-forest SOC but higher R^2 and LCCC for
603 forest SOC (Figure 6). SOC in forest is more abundant and variable compared to SOC in other
604 vegetation types even when climate conditions are similar, which constrains the accuracy of
605 forest SOC estimation. However, the higher R^2 and LCCC mean that all models show higher
606 ability to predict forest SOC using environmental predictors. Forests, given they are less
607 perturbed ecosystems, might afford greater SOC predictability due to the reduced influence of
608 direct anthropogenic disturbances. This stands in contrast to ecosystems like grasslands,
609 shrublands, and woodlands, predominantly situated in Australian rangelands where extensive
610 grazing constitutes the predominant agricultural practice. Primarily, grazing leads to a reduction
611 in soil carbon influx originating from aboveground biomass. Moreover, the cascading effects
612 of grazing extend to potential alterations in plant composition and structural attributes, inducing
613 consequential shifts in litter properties that modulate soil carbon decomposition kinetics (Lunt
614 et al., 2007; Bai and Cotrufo, 2022). This intricate interplay of grazing-induced disturbances
615 introduces a layer of complexity to SOC predictions. The disturbances triggered by grazing
616 manifest in soil carbon pools, leading to a state of disequilibrium rather than adhering to the
617 assumption of SOC convergence toward equilibrium, as embraced in this study's framework.
618 Notably, forests, as relatively undisturbed natural ecosystems, demonstrate a better coherence
619 with the equilibrium assumption, rendering their SOC more amenable to prediction through
620 environmental drivers.

621

622 4.3. Spatial prediction of SOC stocks

623

624 We produced gridded SOC stocks across Australia using the models validated in this study and
625 an ensemble estimate as the average of four models (Figure 7). Among the models, K-means
626 coupled with multiple linear regression produced the largest mean SOC stocks both at



627 continental scale and for all vegetation types. In contrast, random forest and MIMICS with
628 different parameterization approaches produced more conservative SOC stock estimations. The
629 mean terrestrial SOC stocks estimated by random forest and MIMICS are comparable with that
630 estimated by Australian baseline map, which was generated using machine learning algorithm,
631 reporting the mean SOC stocks at 29.7 t/ha with 95% confidence limits of 22.6 and 37.9 t/ha
632 (Viscarra Rossel et al., 2014). However, SOC stocks might be underestimated by these methods
633 because of the scarcity of data from the most productive temperate forest both in the baseline
634 map (Bennett et al., 2020) and in our study. Parameter optimization process of MIMICS and
635 the training process of random forest are greatly affected by data used to train the model. Most
636 SOC observations in this study were sourced from arid and semiarid regions, characterized by
637 limited SOC content. As a result, the models' ability to predict SOC stocks beyond the observed
638 data range is somewhat constrained. PFTs was found to be less important than other
639 environmental factors in driving spatial SOC variations (Figure 3), so it was perhaps not
640 surprising that applying parameters optimized for each plant functional type to the regions with
641 same PFT but broader climate conditions led to inferior results than applying parameters
642 optimized for each environmental group.

643
644 The utilization of linear regression in K-means + MLR generated SOC estimates beyond the
645 range of observations, particularly in eastern Australia where environmental conditions deviate
646 from the training data. The mean SOC stocks estimated by K-means + MLR (38.2 t/ha) are
647 higher than those of the other models employed in this study, and align closely with the mean
648 value 36.2 t/ha reported by Walden et al. (2023) who updated the Australian baseline SOC map
649 (Viscarra Rossel et al., 2014) by incorporating additional SOC observations from forests and
650 coastal marine ecosystems. However, caution is required when interpreting extreme values
651 derived from the K-means + MLR, such as the instance of grassland SOC stocks reaching 601
652 t/ha (Table 3). These values raise concerns about the reliability of this approach when
653 extrapolating out-of-sample. Though there is a positive relationship between NPP and SOC
654 observations in this study, SOC accumulation cannot continuously increase linearly in the
655 regions where environmental conditions seem highly conducive to SOC formation. The greater
656 amount of carbon input in eastern Australia might trigger the acceleration of microbial
657 decomposition because of a priming effect, and lead to a decreased accumulation of SOC stocks
658 (Ren et al., 2022). The existence of SOC saturation also implies that SOC cannot be
659 accumulated without limit (Georgiou et al., 2022; Viscarra Rossel et al., 2023). In light of these
660 complexities, applying linear regression to predict SOC content, especially under the extreme
661 environmental conditions, should be undertaken with care.

662
663 Continentally, higher SOC was estimated for the southwest corner and southeast Australia
664 (Figure 7), aligning with other SOC maps for Australia (Wadoux et al., 2023; Walden et al.,
665 2023). These regions are characterized by lower temperature and higher precipitation, therefore
666 high SOC accumulation appeared because of stimulation of NPP by moisture and the
667 constrained microbial metabolism in low temperatures. Forest has the largest mean SOC stocks
668 ranging from 70.3 to 113.9 t/ha estimated by four models in this study. Around 75% of the forest



669 SOC is from soil under Eucalypt open forest, and mean SOC stocks under this type of forest
670 were estimated to be 87.5 t/ha (63.8 -119.6 t/ha for 95% confidence interval) (Walden et al.,
671 2023). Shrublands are estimated to have the lowest mean SOC stocks, and more than 90% of
672 shrub SOC observations are from soil under Acacia shrubland and Chenopod shrubland, which
673 rank at the bottom of SOC stocks among different vegetation types (Walden et al., 2023). The
674 low SOC in shrubland is probably due to low carbon input because of limited rainfall (MAP <
675 280 mm). Though the mean SOC stocks in non-forest regions are much smaller than that for
676 forest, the greater area of vegetation cover results in considerable total SOC stocks, highlighting
677 the importance of carbon building and maintaining via improved managements in these areas.
678 Greater variability of SOC estimates among different models appears in the regions where SOC
679 stocks are higher (Figure 7). The sparsity of SOC observations is a primary contributor to the
680 uncertainties associated with SOC estimates in these regions, highlighting the importance on
681 continual collection of data to better constrain models' behaviour. This imperative is especially
682 pronounced in regions covered by forests, as forested soils exhibit substantial SOC stocks,
683 amplifying the significance of abundant and accurate data acquisition in these specific
684 ecosystems.

685 5. Conclusion

686
687 We compared the performance of two machine learning models, and one process-based
688 microbial model employing distinct parameterization approaches, to explore the diversity of
689 SOC estimates within a 30 cm soil depth across Australia. Results highlight soil bulk density
690 and MAT as predominant factors governing SOC concentration variations, both on a continental
691 scale and within forest and grassland ecosystems. Conversely, NPP and MAP exhibit greater
692 significance in driving SOC variations within shrubland and woodland soil. Our study
693 underscores the importance of including the influence of appropriate environmental factors in
694 process-based models in different environments.

695
696 Validation results affirm that with appropriate filtering of data (e.g. removing highly managed
697 crop ecosystems) models can predict SOC at a continental scale with reasonably high reliability,
698 achieving explained variances exceeding 80% for out-of-sample test data, with random forest
699 showing highest prediction accuracy. Notably, all models show higher R^2 in prediction of SOC
700 under forest than under non-forest vegetations. MIMICS, with parameters optimized for
701 different environmental clusters, performed better in SOC prediction than MIMICS with
702 parameters optimized for different PFTs, especially in non-forest regions.

703
704 All models broadly agree on the spatial distribution of SOC, with higher SOC stocks
705 concentrated in the southeast and southwest regions of Australia. However, the variations in
706 estimated values need to be acknowledged, particularly in highly productive regions. Among
707 these estimates, K-means algorithm coupled with multiple linear regression yields the highest
708 mean SOC stocks estimate, while the MIMICS-PFT model generates the most conservative
709 estimate. Considerable disagreement of the maximum and minimum SOC stock values



710 predicted by all models exists partly because models are less constrained by observations in
711 these environments, highlighting the need for continued observational campaigns.

712

713 Our investigation has revealed significant disparities in estimated SOC stocks when different
714 methodologies were employed. This highlights the need for a critical re-evaluation of land
715 management strategies that heavily depend on SOC estimates derived from a single approach.
716 The incorporation of an ensemble of SOC estimates is more likely to effectively capture
717 elements of the uncertainty associated with SOC estimations, providing a more robust basis for
718 informing strategies in soil carbon management and climate change mitigation.

719 Code availability

720

721 Source Code of vertically resolved MIMICS can be accessed at the CSIRO data portal
722 <https://doi.org/10.25919/843a-w584> (Wang et al., 2021). Codes for data analysis and machine
723 learning can be accessed by contacting the correspondence author.

724 Data availability

725

726 The SOC observations from VR dataset are not publicly available but are available from
727 Raphael A. Viscarra Rossel (r.viscarra-rossel@curtin.edu.au) on reasonable request. All other
728 data used in this study are publicly accessible and the specific references of these databases are
729 provided in Section 2.4.

730 Author contribution

731

732 Conceptualization: LW, GA, Y-PW, AP; Methodology: LW, GA, Y-PW; Investigation: LW,
733 RAVR; Formal analysis and Visualization: LW; Writing-original draft preparation: LW;
734 Writing-review & editing: LW, GA, Y-PW, AP, RAVR.

735 Competing interests

736

737 The co-author Raphael A. Viscarra Rossel is a member of the editorial board of SOIL.

738 Acknowledgements

739

740 LW thanks the China Scholarship Council and the University of New South Wales for financial
741 support during her PhD study. RAVR and Y-PW thank the Australian Research Council's
742 Discovery Projects scheme (project DP210100420) for funding. LW, GA and AP thank the ARC
743 Centre of Excellence for Climate Extremes for supporting this work (CE170100023).

744

745

746



747 Reference

748

749 Abramoff, R. Z., Guenet, B., Zhang, H., Georgiou, K., Xu, X., Viscarra Rossel, R. A., Yuan, W.
750 and Ciais, P.: Improved global-scale predictions of soil carbon stocks with Millennial Version
751 2. *Soil Biol Biochem*, 164, 108466, <https://doi.org/10.1016/j.soilbio.2021.108466>, 2022.

752 Abs, E. and Ferrière, R.: Modeling microbial dynamics and heterotrophic soil respiration: Effect
753 of climate change. *Biogeochemical cycles: ecological drivers and environmental impact*,
754 103-129, <https://doi.org/10.1002/9781119413332.ch5>, 2020.

755 Adhikari, K., Mishra, U., Owens, P., Libohova, Z., Wills, S., Riley, W., Hoffman, F. and Smith,
756 D.: Importance and strength of environmental controllers of soil organic carbon changes with
757 scale. *Geoderma*, 375, 114472, <https://doi.org/10.1016/j.geoderma.2020.114472>, 2020.

758 Bai, Y. and Cotrufo, M. F.: Grassland soil carbon sequestration: Current understanding,
759 challenges, and solutions. *Science*, 377, 603-608, doi: 10.1126/science.abo2380, 2022.

760 Bennett, L. T., Hinko-Najera, N., Aponte, C., Nitschke, C. R., Fairman, T. A., Fedrigo, M. and
761 Kasel, S.: Refining benchmarks for soil organic carbon in Australia's temperate forests.
762 *Geoderma*, 368, 114246, <https://doi.org/10.1016/j.geoderma.2020.114246>, 2020.

763 Bossio, D., Cook-Patton, S., Ellis, P., Fargione, J., Sanderman, J., Smith, P., Wood, S., Zomer,
764 R., Von Unger, M. and Emmer, I.: The role of soil carbon in natural climate solutions. *Nat*
765 *Sustain*, 3, 391-398, <https://doi.org/10.1038/s41893-020-0491-z>, 2020.

766 Breiman, L.: Random forests. *Machine learning*, 45, 5-32,
767 <https://doi.org/10.1023/A:1010933404324>, 2001.

768 Bronick, C. J. and Lal, R.: Soil structure and management: a review. *Geoderma*, 124, 3-22,
769 <https://doi.org/10.1016/j.geoderma.2004.03.005>, 2005.

770 Cranko Page, J., Abramowitz, G., De Kauwe, M. G. and Pitman, A. J.: Are plant functional
771 types fit for purpose? *Geophys Res Lett*, 2023 (accepted).

772 Chandel, A. K., Jiang, L. and Luo, Y.: Microbial Models for Simulating Soil Carbon Dynamics:
773 A Review. *J Geophys Res-Bioge*, e2023JG007436, <https://doi.org/10.1029/2023JG007436>,
774 2023.

775 De Deyn, G. B., Cornelissen, J. H. and Bardgett, R. D.: Plant functional traits and soil carbon
776 sequestration in contrasting biomes. *Ecol Lett*, 11, 516-531, <https://doi.org/10.1111/j.1461-0248.2008.01164.x>, 2008.

778 Debeer, D. and Strobl, C.: Conditional permutation importance revisited. *BMC bioinformatics*,
779 21, 1-30, <https://doi.org/10.1186/s12859-020-03622-2>, 2020.

780 Doetterl, S., Stevens, A., Six, J., Merckx, R., Van Oost, K., Casanova Pinto, M., Casanova-
781 Katny, A., Muñoz, C., Boudin, M. and Zagal Venegas, E.: Soil carbon storage controlled by
782 interactions between geochemistry and climate. *Nat Geosci*, 8, 780-783,
783 <https://doi.org/10.1038/ngeo2516>, 2015.

784 Don, A., Schumacher, J., Scherer-Lorenzen, M., Scholten, T. and Schulze, E.-D.: Spatial and
785 vertical variation of soil carbon at two grassland sites—implications for measuring soil
786 carbon stocks. *Geoderma*, 141, 272-282, <https://doi.org/10.1016/j.geoderma.2007.06.003>,
787 2007.



- 788 Duan, Q., Gupta, V. K. and Sorooshian, S.: Shuffled complex evolution approach for effective
789 and efficient global minimization. *J Optim Theory Appl*, 76: 501-521,
790 <https://doi.org/10.1007/BF00939380>, 1993.
- 791 Famiglietti, C. A., Worden, M., Quetin, G. R., Smallman, T. L., Dayal, U., Bloom, A. A.,
792 Williams, M. and Konings, A. G.: Global net biome CO₂ exchange predicted comparably
793 well using parameter–environment relationships and plant functional types. *Glob Change*
794 *Biol*, 29, 2256-2273, <https://doi.org/10.1111/gcb.16574>, 2023.
- 795 Faucon, M.-P., Houben, D. and Lambers, H.: Plant functional traits: soil and ecosystem services.
796 *Trends Plant Sci*, 22, 385-394, <https://doi.org/10.1016/j.tplants.2017.01.005>, 2017.
- 797 Georgiou, K., Malhotra, A., Wieder, W. R., Ennis, J. H., Hartman, M. D., Sulman, B. N., Berhe,
798 A. A., Grandy, A. S., Kyker-Snowman, E. and Lajtha, K.: Divergent controls of soil organic
799 carbon between observations and process-based models. *Biogeochemistry*, 156, 5-17,
800 <https://doi.org/10.1007/s10533-021-00819-2>, 2021.
- 801 Georgiou, K., Jackson, R. B., Vindušková, O., Abramoff, R. Z., Ahlström, A., Feng, W., Harden,
802 J. W., Pellegrini, A. F., Polley, H. W. and Soong, J. L.: Global stocks and capacity of mineral-
803 associated soil organic carbon. *Nat Commun*, 13, 3797, <https://doi.org/10.1038/s41467-022-31540-9>, 2022.
- 805 Grace, P. R., Post, W. M. and Hennessy, K.: The potential impact of climate change on
806 Australia's soil organic carbon resources. *Carbon Balance Manag*, 1, 1-10,
807 <https://doi.org/10.1186/1750-0680-1-14>, 2006.
- 808 Grundy, M., Viscarra Rossel, R. A., Searle, R., Wilson, P., Chen, C. and Gregory, L.: Soil and
809 landscape grid of Australia. *Soil Res*, 53, 835-844, <https://doi.org/10.1071/SR15191>, 2015.
- 810 Guo, Z., Adhikari, K., Chellasamy, M., Greve, M. B., Owens, P. R. and Greve, M. H.: Selection
811 of terrain attributes and its scale dependency on soil organic carbon prediction. *Geoderma*,
812 340, 303-312, <https://doi.org/10.1016/j.geoderma.2019.01.023>, 2019.
- 813 Heung, B., Ho, H. C., Zhang, J., Knudby, A., Bulmer, C. E. and Schmidt, M. G.: An overview
814 and comparison of machine-learning techniques for classification purposes in digital soil
815 mapping. *Geoderma*, 265, 62-77, <https://doi.org/10.1016/j.geoderma.2015.11.014>, 2016.
- 816 Hobley, E., Wilson, B., Wilkie, A., Gray, J. and Koen, T.: Drivers of soil organic carbon storage
817 and vertical distribution in Eastern Australia. *Plant Soil*, 390, 111-127,
818 <https://doi.org/10.1007/s11104-015-2380-1>, 2015.
- 819 Hobley, E. U., Baldock, J. and Wilson, B.: Environmental and human influences on organic
820 carbon fractions down the soil profile. *Agric Ecosyst Environ*, 223, 152-166,
821 <https://doi.org/10.1016/j.agee.2016.03.004>, 2016.
- 822 Jeffrey, S. J., Carter, J. O., Moodie, K. B. and Beswick, A. R.: Using spatial interpolation to
823 construct a comprehensive archive of Australian climate data. *Environ Model Softw*, 16, 309-
824 330, [https://doi.org/10.1016/S1364-8152\(01\)00008-1](https://doi.org/10.1016/S1364-8152(01)00008-1), 2001.
- 825 Jenny, H.: Factors of soil formation: a system of quantitative pedology, Courier Corporation,
826 <https://doi.org/10.2134/agronj1941.00021962003300090016x>, 1994.
- 827 Jobbágy, E. G. and Jackson, R. B.: The Vertical Distribution of Soil Organic Carbon and Its
828 Relation to Climate and Vegetation. *Ecol Appl*, 10, 423-436, [https://doi.org/10.1890/1051-0761\(2000\)010\[0423:TVDOSO\]2.0.CO;2](https://doi.org/10.1890/1051-0761(2000)010[0423:TVDOSO]2.0.CO;2), 2000.



- 830 Keskin, H., Grunwald, S. and Harris, W. G.: Digital mapping of soil carbon fractions with
831 machine learning. *Geoderma*, 339, 40-58, <https://doi.org/10.1016/j.geoderma.2018.12.037>,
832 2019.
- 833 Lamichhane, S., Kumar, L. and Wilson, B.: Digital soil mapping algorithms and covariates for
834 soil organic carbon mapping and their implications: A review. *Geoderma*, 352, 395-413,
835 <https://doi.org/10.1016/j.geoderma.2019.05.031>, 2019.
- 836 Lawrence, I. and Lin, K.: A concordance correlation coefficient to evaluate reproducibility.
837 *Biometrics*, 45, 255-268, <https://doi.org/10.2307/2532051>, 1989.
- 838 Lee, J., Viscarra Rossel, R. A., Zhang, M., Luo, Z. and Wang, Y. P.: Assessing the response of
839 soil carbon in Australia to changing inputs and climate using a consistent modelling
840 framework. *Biogeosciences*, 18, 5185-5202, <https://doi.org/10.5194/bg-18-5185-2021>, 2021.
- 841 Lefèvre, C., Rekik, F., Alcantara, V. and Wiese, L.: Soil organic carbon: the hidden potential,
842 Food and Agriculture Organization of the United Nations (FAO), [http://www.fao.org/3/a-](http://www.fao.org/3/a-i6937e.pdf)
843 [i6937e.pdf](http://www.fao.org/3/a-i6937e.pdf), 2017.
- 844 Lehmann, J. and Kleber, M.: The contentious nature of soil organic matter. *Nature*, 528, 60-68,
845 <https://doi.org/10.1038/nature16069>, 2015.
- 846 Liang, Z., Chen, S., Yang, Y., Zhou, Y. and Shi, Z.: High-resolution three-dimensional mapping
847 of soil organic carbon in China: Effects of SoilGrids products on national modeling. *Sci Total*
848 *Environ*, 685, 480-489, <https://doi.org/10.1016/j.scitotenv.2019.05.332>, 2019.
- 849 Lobsey, C. and Viscarra Rossel, R.: Sensing of soil bulk density for more accurate carbon
850 accounting. *Eur J Soil Sci*, 67, 504-513, <https://doi.org/10.1111/ejss.12355>, 2016.
- 851 Lorenz, K., Lal, R. and Ehlers, K.: Soil organic carbon stock as an indicator for monitoring land
852 and soil degradation in relation to United Nations' Sustainable Development Goals. *Land*
853 *Degrad Dev*, 30, 824-838, <https://doi.org/10.1002/ldr.3270>, 2019.
- 854 Lunt, I. D., Eldridge, D. J., Morgan, J. W. and Witt, G. B.: A framework to predict the effects
855 of livestock grazing and grazing exclusion on conservation values in natural ecosystems in
856 Australia. *Australian Journal of Botany*, 55, 401-415, <https://doi.org/10.1071/BT06178>,
857 2007.
- 858 Luo, Y., Ahlström, A., Allison, S. D., Batjes, N. H., Brovkin, V., Carvalhais, N., Chappell, A.,
859 Ciais, P., Davidson, E. A. and Finzi, A.: Toward more realistic projections of soil carbon
860 dynamics by Earth system models. *Global Biogeochem Cycles*, 30, 40-56,
861 <https://doi.org/10.1002/2015GB005239>, 2016.
- 862 Luo, Z., Wang, E. and Sun, O. J.: Soil carbon change and its responses to agricultural practices
863 in Australian agro-ecosystems: a review and synthesis. *Geoderma*, 155, 211-223,
864 <https://doi.org/10.1016/j.geoderma.2009.12.012>. 2010.
- 865 McBratney, A. B., Santos, M. M. and Minasny, B.: On digital soil mapping. *Geoderma*, 117, 3-
866 52, [https://doi.org/10.1016/S0016-7061\(03\)00223-4](https://doi.org/10.1016/S0016-7061(03)00223-4), 2003.
- 867 Minasny, B., McBratney, A. B., Malone, B. P. and Wheeler, I.: Digital mapping of soil carbon.
868 *Advances in agronomy*, 118, 1-47, <https://doi.org/10.1016/B978-0-12-405942-9.00001-3>,
869 2013.



- 870 Mishra, U. and Riley, W.: Scaling impacts on environmental controls and spatial heterogeneity
871 of soil organic carbon stocks. *Biogeosciences*, 12, 3993-4004, [https://doi.org/10.5194/bg-12-](https://doi.org/10.5194/bg-12-3993-2015)
872 3993-2015, 2015.
- 873 Mokany, K., Raison, R. J. and Prokushkin, A. S.: Critical analysis of root: shoot ratios in
874 terrestrial biomes. *Glob Change biol*, 12, 84-96, [https://doi.org/10.1111/j.1365-](https://doi.org/10.1111/j.1365-2486.2005.001043.x)
875 2486.2005.001043.x, 2006.
- 876 Nyaupane, K., Mishra, U., Tao, F., Yeo, K., Riley, W. J., Hoffman, F. M. and Gautam, S.:
877 Observational benchmarks inform representation of soil organic carbon dynamics in land
878 surface models. *Biogeosci Discuss*, 2023, 1-28, <https://doi.org/10.5194/bg-2023-50>, 2023.
- 879 Panchal, P., Preece, C., Penuelas, J. and Giri, J.: Soil carbon sequestration by root exudates.
880 *Trends Plant Sci*, 27, 749-757, <https://doi.org/10.1016/j.tplants.2022.04.009>, 2022.
- 881 Poulter, B., MacBean, N., Hartley, A., Khlystova, I., Arino, O., Betts, R., Bontemps, S.,
882 Boettcher, M., Brockmann, C. and Defourny, P.: Plant functional type classification for earth
883 system models: results from the European Space Agency's Land Cover Climate Change
884 Initiative. *Geosci Model Dev*, 8, 2315-2328, <https://doi.org/10.5194/gmd-8-2315-2015>,
885 2015.
- 886 Ren, C., Mo, F., Zhou, Z., Bastida, F., Delgado-Baquerizo, M., Wang, J., Zhang, X., Luo, Y.,
887 Griffis, T. J. and Han, X.: The global biogeography of soil priming effect intensity. *Global*
888 *Ecol Biogeogr*, 31, 1679-1687, <https://doi.org/10.1111/geb.13524>, 2022.
- 889 Rossel, R. V., Chen, C., Grundy, M., Searle, R., Clifford, D. and Campbell, P. The Australian
890 three-dimensional soil grid: Australia's contribution to the GlobalSoilMap project. *Soil Res*,
891 53, 845-864, <https://doi.org/10.1071/SR14366>, 2015.
- 892 Rumpel, C., Amiraslani, F., Koutika, L.-S., Smith, P., Whitehead, D. and Wollenberg, E.: Put
893 more carbon in soils to meet Paris climate pledges, *Nature*, 564, 32-34,
894 <https://doi.org/10.1038/d41586-018-07587-4>, 2018.
- 895 Six, J., Conant, R. T., Paul, E. A. and Paustian, K.: Stabilization mechanisms of soil organic
896 matter: Implications for C-saturation of soils. *Plant Soil*, 241, 155-176,
897 <https://doi.org/10.1023/A:1016125726789>, 2002.
- 898 Smith, P.: Soil carbon sequestration and biochar as negative emission technologies. *Glob*
899 *Change Biol*, 22, 1315-1324, <https://doi.org/10.1111/gcb.13178>, 2016.
- 900 Stockmann, U., Padarian, J., McBratney, A., Minasny, B., de Brogniez, D., Montanarella, L.,
901 Hong, S. Y., Rawlins, B. G. and Field, D. J.: Global soil organic carbon assessment. *Glob*
902 *Food Sec*, 6, 9-16, <https://doi.org/10.1016/j.gfs.2015.07.001>, 2015.
- 903 Stockmann, U., Adams, M. A., Crawford, J. W., Field, D. J., Henakaarchchi, N., Jenkins, M.,
904 Minasny, B., McBratney, A. B., De Courcelles, V. d. R. and Singh, K.: The knowns, known
905 unknowns and unknowns of sequestration of soil organic carbon. *Agric Ecosyst Environ*,
906 164, 80-99, <https://doi.org/10.1016/j.agee.2012.10.001>, 2013.
- 907 Terrer, C., Phillips, R. P., Hungate, B. A., Rosende, J., Pett-Ridge, J., Craig, M. E., van
908 Groenigen, K. J., Keenan, T. F., Sulman, B. N., Stocker, B. D., Reich, P. B., Pellegrini, A. F.
909 A., Pendall, E., Zhang, H., Evans, R. D., Carrillo, Y., Fisher, J. B., Van Sundert, K., Vicca, S.
910 and Jackson, R. B.: A trade-off between plant and soil carbon storage under elevated CO₂.
911 *Nature*, 591, 599-603, <https://doi.org/10.1038/s41586-021-03306-8>, 2021.



- 912 Todd-Brown, K., Randerson, J., Hopkins, F., Arora, V., Hajima, T., Jones, C., Shevliakova, E.,
913 Tjiputra, J., Volodin, E. and Wu, T.: Changes in soil organic carbon storage predicted by Earth
914 system models during the 21st century. *Biogeosciences*, 11, 2341-2356,
915 <https://doi.org/10.5194/bg-11-2341-2014>, 2014.
- 916 Todd-Brown, K. E., Randerson, J. T., Post, W. M., Hoffman, F. M., Tarnocai, C., Schuur, E. A.
917 and Allison, S. D.: Causes of variation in soil carbon simulations from CMIP5 Earth system
918 models and comparison with observations. *Biogeosciences*, 10, 1717-1736,
919 <https://doi.org/10.5194/bg-10-1717-2013>, 2013.
- 920 Viscarra Rossel, R. A., Webster, R., Bui, E. N. and Baldock, J. A.: Baseline map of organic
921 carbon in Australian soil to support national carbon accounting and monitoring under climate
922 change. *Glob Change Biol*, 20, 2953-2970, <https://doi.org/10.1111/gcb.12569>, 2014.
- 923 Viscarra Rossel, R. A., Chen, C., Grundy, M. J., Searle, R., Clifford, D. and Campbell, P. H.:
924 The Australian three-dimensional soil grid: Australia's contribution to the GlobalSoilMap
925 project. *Soil Res*, 53, 845-864, <https://doi.org/10.1071/SR14366>, 2015.
- 926 Viscarra Rossel, R. A., Lee, J., Behrens, T., Luo, Z., Baldock, J. and Richards, A.: Continental-
927 scale soil carbon composition and vulnerability modulated by regional environmental
928 controls. *Nat Geosci*, 12, 547-552, <https://doi.org/10.1038/s41561-019-0373-z>, 2019.
- 929 Viscarra Rossel, R. A., Webster, R., Zhang M., Shen, Z., Dixon, K., Wang, Y. P., Walden, L.:
930 How much organic carbon could the soil store? The carbon sequestration potential of
931 Australian soil. *Glob Change Biol*, 30, e17053, <https://doi.org/10.1111/gcb.17053>, 2023.
- 932 Wadoux, A. M. J., Román Dobarco, M., Malone, B., Minasny, B., McBratney, A. B. and Searle,
933 R.: Baseline high-resolution maps of organic carbon content in Australian soils. *Sci Data*, 10,
934 181, <https://doi.org/10.1038/s41597-023-02056-8>, 2023.
- 935 Walden, L., Serrano, O., Zhang, M., Shen, Z., Sippo, J. Z., Bennett, L. T., Maher, D. T.,
936 Lovelock, C. E., Macreadie, P. I. and Gorham, C.: Multi-scale mapping of Australia's
937 terrestrial and blue carbon stocks and their continental and bioregional drivers. *Commun*
938 *Earth Environ*, 4, 189, <https://doi.org/10.1038/s43247-023-00838-x>, 2023.
- 939 Wang, B., Waters, C., Orgill, S., Gray, J., Cowie, A., Clark, A. and Li Liu, D.: High resolution
940 mapping of soil organic carbon stocks using remote sensing variables in the semi-arid
941 rangelands of eastern Australia. *Sci Total Environ*, 630, 367-378,
942 <https://doi.org/10.1016/j.scitotenv.2018.02.204>, 2018a.
- 943 Wang, B., Gray, J. M., Waters, C. M., Anwar, M. R., Orgill, S. E., Cowie, A. L., Feng, P. and Li
944 Liu, D.: Modelling and mapping soil organic carbon stocks under future climate change in
945 south-eastern Australia. *Geoderma*, 405, 115442,
946 <https://doi.org/10.1016/j.geoderma.2021.115442>, 2022.
- 947 Wang, B., Waters, C., Orgill, S., Cowie, A., Clark, A., Li Liu, D., Simpson, M., McGowen, I.
948 and Sides, T.: Estimating soil organic carbon stocks using different modelling techniques in
949 the semi-arid rangelands of eastern Australia. *Ecol Indic*, 88, 425-438,
950 <https://doi.org/10.1016/j.ecolind.2018.01.049>, 2018b.
- 951 Wang, Y. P., Zhang, H., Ciais, P., Goll, D., Huang, Y., Wood, J. D., Ollinger, S. V., Tang, X. and
952 Prescher, A. K.: Microbial activity and root carbon inputs are more important than soil carbon



- 953 diffusion in simulating soil carbon profiles. *J Geophys Res Biogeosci*, 126, e2020JG006205,
954 <https://doi.org/10.1029/2020JG006205>, 2021.
- 955 Wieder, W., Grandy, A., Kallenbach, C., Taylor, P. and Bonan, G.: Representing life in the Earth
956 system with soil microbial functional traits in the MIMICS model. *Geosci Model Dev*, 8,
957 1789-1808, <https://doi.org/10.5194/gmd-8-1789-2015>, 2015.
- 958 Wiesmeier, M., Barthold, F., Spörlein, P., Geuß, U., Hangen, E., Reischl, A., Schilling, B.,
959 Angst, G., von Lützw, M. and Kögel-Knabner, I.: Estimation of total organic carbon storage
960 and its driving factors in soils of Bavaria (southeast Germany). *Geoderma Regional*, 1, 67-
961 78, <https://doi.org/10.1016/j.geodrs.2014.09.001>, 2014.
- 962 Wiesmeier, M., Urbanski, L., Hobbey, E., Lang, B., von Lützw, M., Marin-Spiotta, E., van
963 Wesemael, B., Rabot, E., Ließ, M. and Garcia-Franco, N.: Soil organic carbon storage as a
964 key function of soils-A review of drivers and indicators at various scales. *Geoderma*, 333,
965 149-162, <https://doi.org/10.1016/j.geoderma.2018.07.026>, 2019.
- 966 Wynn, J. G., Bird, M. I., Vellen, L., Grand-Clement, E., Carter, J. and Berry, S. L.: Continental-
967 scale measurement of the soil organic carbon pool with climatic, edaphic, and biotic controls.
968 *Global Biogeochem Cycles*, 20, <https://doi.org/10.1029/2005GB002576>, 2006.
- 969 Zhang, H., Goll, D. S., Wang, Y. P., Ciais, P., Wieder, W. R., Abramoff, R., Huang, Y., Guenet,
970 B., Prescher, A. K. and Viscarra Rossel, R. A.: Microbial dynamics and soil physicochemical
971 properties explain large-scale variations in soil organic carbon. *Glob Change Biol*, 26, 2668-
972 2685, <https://doi.org/10.1111/gcb.14994>, 2020.

973